Decay of Shock Perturbations: A Geometrical Shock Dynamics Study

Aliou Sow*, Yazid Amor, and Matei I. Radulescu

Department of Mechanical Engineering, University of Ottawa, 161 Louis Pasteur, Ottawa, ON, K1N6N5, Canada

1 Introduction

We are concerned with the problem of decay of perturbations on a lead shock wave in an inert gas. This problem arises in shock tubes, whereby the non-ideal burst of the diaphragm gives rise to perturbations on the shock, which subsequently decay with time as the shock propagates. The lack of planarity in the lead shock is also important when shock tubes are used to study chemical kinetics, as local hotspots can arise in regions when a stronger shock reflects on a wall. In the context of deflagration to detonation transition (DDT), for example, the final stages involve a turbulent flame driving a shock wave. In the presence of obstacles, the shock is perturbed, and these perturbations affect the flame dynamics and create hot-spots conducive to detonation transition. We are thus concerned with determining the decay rate of perturbations on a shock wave, a problem that commonly arises in many practical problems.

Owing to non-linearities of gasdynamics, perturbations to the lead shock take the form of triple points. We wish to establish the decay rate of triple points. To date, this fundamental problem has received little attention in the literature. Bowman [1] has determined experimentally in round shock tubes that such Mach reflections decay slowly as $t^{1/2}$ after passing an obstacle, in good accord with the acoustic theory of Freeman [2] . When the shock is driven by a corrugated piston, numerical simulations revealed a similar $t^{1/2}$ decay [3], although ambiguities in the data reduction persist. Other than direct simulation [3, 4], only two approximate models can predict the Mach shock decaying solutions, although these have not yet been used to answer this question. An approximate model formulated by Clavin [5] in the Newtonian limit (strong shocks, ratio of specific heats approaching unity), can be used to answer this question for the planar case; it was found successful in predicting the shock shape in 2D [6]. The other approximate model to predict the shock evolution is Whitham's Geometrical Shock Dynamics (GSD) method [7]. It can be simply generalized to treat both 2D and 3D cases, as it evolves the lead shock and its disturbances as a level set. The GSD approach to this problem has previously been demonstrated by Mostert et al. [8] as an extension to Schwendeman's simple method [9]. This study will focus mainly on the direct numerical and the GSD method, as they can treat both an axi-symmetric and planar geometries of interest. We thus address the problem of perturbations on a lead shock numerically, by solving the Euler equations, and semi-analytically, using the GSD framework, seeking an analytical solution to this problem.

Correspondence to: asow2@uottawa.ca

2 Geometrical Shock Dynamics Formalism: Equations and Numerical Method

In this section, we provide a brief overview of the mathematical and numerical modeling employed. The formalism utilized is based on the work of Schwendeman [9], wherein the motion of shock waves is determined through geometrical shock dynamics. The governing equations are as follows:

$$\nabla \cdot \left(\left(\frac{\mathrm{M}}{A} \right) \nabla \alpha \right) = 0, \quad \mathrm{M} = \frac{1}{\nabla \alpha}, \quad A = f(\mathrm{M}),$$

where M represents the Mach number of the leading shock, and α defines the position x of the leading shock as a function of time. The relation $A = f(\mathrm{M})$ corresponds to the A-M relation, which characterizes the connection between the area A of the ray tube and the local Mach number M. In this study, we will apply Whitham's A-M relation [7]. The governing equation constitutes a second-order partial differential equation of hyperbolic type, which facilitates the natural formation of discontinuities, such as shock-shock interactions. The governing equation can be solved in both two-dimensional and three-dimensional spaces. For the purposes of this work, we will restrict our analysis to two dimensions. The initial conditions are described as follows:

$$\alpha = 0, \quad \frac{\partial \alpha}{\partial n} = 1/\mathrm{M}_0 \quad \text{on} \quad S(x) = 0,$$

where $S(x) = 0$ defines the initial shock shape, and n represents the inward unit normal to the surface $S(x)$. M_0 is the initial Mach number, which has known values at the start of the simulation, $t = 0$.

The governing equations are supplemented by boundary conditions. Along the channel walls, zero normal derivatives are imposed, and no boundary conditions are set at the channel exit.

We are focused on the propagation of shock waves within a straight rectangular channel, where the height spans from $y = 0$ to $y = 1$. The governing equations for the flow dynamics are therefore expressed as:

$$\frac{\partial Fu}{\partial x} + \frac{\partial Fv}{\partial y} = 0, \quad u = \frac{\partial \alpha}{\partial x}, \quad v = \frac{\partial \alpha}{\partial y}, \quad \mathrm{M} = \left(u^2 + v^2\right)^{-0.5}, \quad A = f(\mathrm{M}), \quad \text{and} \quad F = \frac{\mathrm{M}}{A},$$

where u and v are inversely proportional to the velocity components in the x and y directions, respectively, and are related to the shock location function α. All variables are expressed as functions of α. Furthermore, Whitham's A-M relation is given by the following equation:

$$A = \frac{g(\mathrm{M})}{g(\mathrm{M}_0)}, \quad g(\mathrm{M}) = \frac{\mathrm{M}}{\mathrm{M}^2 - 1} \left(1 + \frac{2}{\gamma + 1} \frac{1 - \mu^2}{\mu} \right) \left(1 + 2\mu + \frac{1}{\mathrm{M}^2} \right) = 0, \quad \mu^2 = \frac{(\gamma - 1)\mathrm{M}^2 + 2}{2\gamma \mathrm{M}^2 - (\gamma - 1)},$$

where γ is the ratio of specific heats, which is set to 1.376 in this study.

To solve these equations numerically, we discretize the domain in both the x- and y-directions using i and j nodes, respectively. A root-finding method is employed to obtain the solution for each node in the domain at a given i, i.e., for all $\alpha_{i,j}$ where j ranges from 0 to N_y, the number of grid points in the y-direction.

In order to accurately capture shock interactions, particularly shock-shock collisions, a numerical viscosity is introduced to the right-hand side of the second-order partial differential equation, as described in [9]. This technique helps to stabilize the solution and resolve the sharp gradients that occur across shock fronts, ensuring the proper formation and evolution of discontinuities in the flow. Readers are encouraged to refer to the paper by Schwendeman [9] for further details.

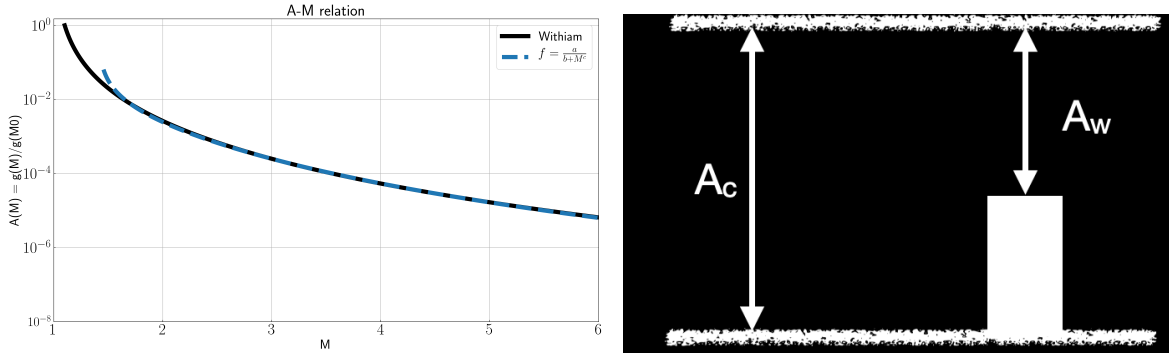

Figure 1: Left subfigure: Whitham's A-M relation and the fitting function used in the GSD numerical simulations; Right subfigure: Numerical setup defining the Mach number at the center of the channel and at the wall, which are used to determine the magnitude of the starting shock perturbations.

To enhance computational efficiency, a fitting function of the form $A = \frac{0.08}{\mathrm{M}^{5.27}-6}$ was employed in place of Whitham's A-M relation. The accuracy of this fitting function is validated in the left subfigure of Figure 1, where it exhibits a satisfactory agreement with the theoretical results.

To define the magnitude of the initial perturbations, we utilize the A-M relation. When a planar shock wave of given strength M_c encounters an obstacle, as illustrated schematically in the right subfigure of Figure 1, the shock strength over the obstacle, denoted as M_w, can be determined using the A-M relation. Once the magnitude of the initial perturbations is established, a cosine function is employed to distribute the shock strength at the entrance of the channel, $x = 0$. The initial perturbations are then defined as follows:

$$\frac{1}{\mathrm{M}_0} = \frac{1}{2}\left(\frac{\mathrm{M}_c + \mathrm{M}_w}{\mathrm{M}_c\mathrm{M}_w}\right)\left(1 + \frac{\mathrm{M}_c - \mathrm{M}_w}{\mathrm{M}_c + \mathrm{M}_w} cos(2\pi y)\right)$$

The defined Mach number distribution enables shock focusing within the straight channel.

3 Results

Figure 2 illustrates the shock positions at selected times within the channel, with the figure color-coded to reflect the Mach number of the leading shock. Shortly after the simulation begins, the shock focuses, leading to the formation of shock-shocks within a distance of less than one unit length. The trajectories of these shock-shocks exhibit a diamond-like structure, resembling the cellular patterns observed in gaseous detonation shock waves. As the leading shock front propagates downstream, its curvature progressively diminishes. Concurrently, the shock strength decreases, and the trajectories of the shock-shocks become increasingly less pronounced.

With the Mach number map established, we now examine in greater detail the diminishing shock strength. We record the shock strength along both the top wall and the centerline of the channel, with the results shown in Figure 3. Along the top wall, the shock begins with its highest strength, which rapidly decreases until a shock-shock interaction occurs near the wall, temporarily increasing the shock strength to a new peak. However, this peak is lower than the initial Mach number peak. This process repeats over time, with the shock strength progressively fading, corresponding to a flattening of the shock's curvature, as previously noted. A similar behavior is observed when analyzing the centerline data, though the shock at the centerline initially exhibits the lowest strength. The first shock-shock interaction recorded along the centerline corresponds to the highest Mach number observed, as shown in the lower panel of Figure 3. The periodic decay of the shock resembles the behavior of N-waves.

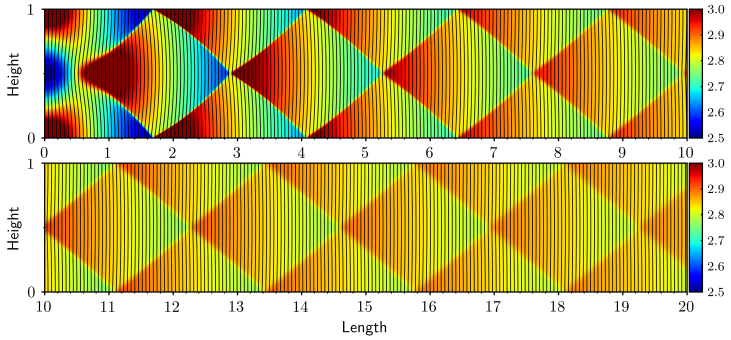

Figure 2: Contours of constant α (denoted by the black lines) represent the shock positions within the channel. The map is color-coded according to the Mach number of the leading shock. The bottom figure serves as a continuation of the top figure.

To derive the scaling law for shock strength decay, we analyze the Mach number fluctuations, as shown in the top panel of Figure 3. In the log-log scale, we seek a power law that passes through the maximum shock strength peaks. The first three peaks are excluded, as they are associated with the formation of shock-shocks and may be influenced by initial numerical perturbations. The power law takes the form $\mathrm{M}' = A/x^B$, where the global envelope of the shock (i.e., the envelope of the peak shock strengths) decays according to $1/x$, as summarized in Table 1. A and B are constants.

Table 1: Shock decay law: $\mathrm{M}' = A/x^B$; A and B are constants.

Top wall	A= 0.837	B=1.032
Centreline wall	A= 0.778	B=1.005

We also investigate the internal decay of shock strength within the system. To model this internal decay, we employ a linearly decaying function, which periodically decreases with respect to the distance, represented by the equation:

$$\mathrm{M}(x) = A_j x + B_j$$

where $\mathrm{M}(x)$ is the shock strength at position x, and A_j and B_j are constants that define the magnitude and offset of the decay, respectively. These constants are empirically determined using the global decay law that characterizes the overall decay profile of the shock. This allows us to establish a quantitative measure of the internal decay's magnitude. A graphical representation of this decay law is provided in Figure 4. The validation of the linear decay model is achieved by comparing it to the actual behavior of the observed N-waves, which typically exhibit a nonlinear decay profile. The linearly decaying approximation proves to be a reasonable model for these waves under the given conditions. To substantiate this approximation, we compare the probability density function (PDF) of the GSD simulation against the proposed analytical decay rate. The results of this comparison are shown in Figure 5, where the alignment of the theoretical decay rate with GSD confirms the adequacy of the linear approximation.

4 Discussion and Future works

This study provides valuable insights into the dynamics of shock decay within a confined channel. Quantitative analysis reveals that the shock decay follows a nearly linear trend with distance. As shown in Figure 5, the comparison between the analytical decay rate and the GSD probability density function

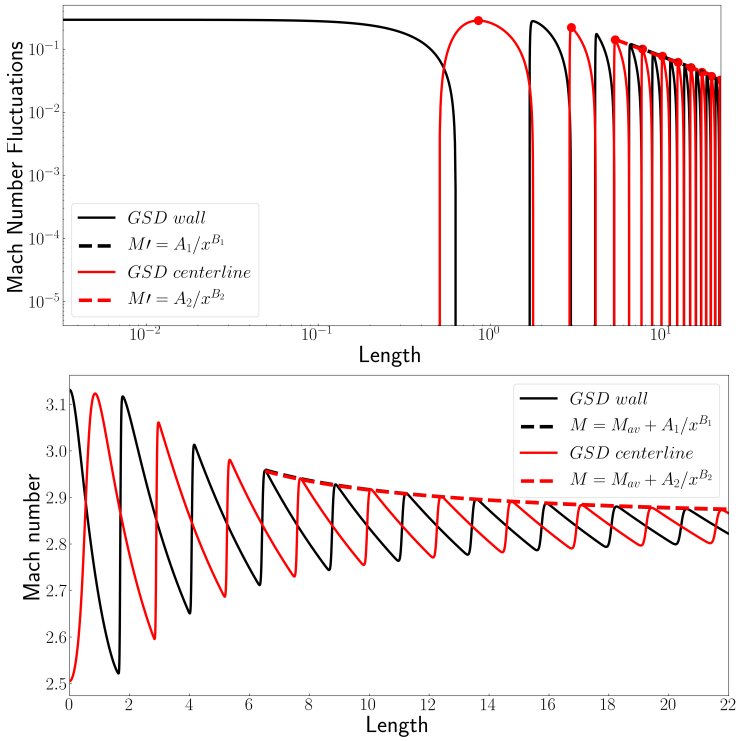

Figure 3: Mach number fluctuations along the the top wall (black solid line) and the centerline (red solid line) and dotted lines fitting functions; Mach number along the top wall (black solid line)and the centerline (red solid line) and corresponding fitting functions.

(PDF) supports the use of a linear decay model, despite nonlinear effects. The observed shock-shock interactions and the resulting changes in shock strength are consistent with the expected behavior of N-waves, indicating two families of N-waves propagating within the channel. Their interaction produces a global decay of $1/x$. The proposed linearly decaying internal model effectively approximates shock perturbations and provides a useful framework for future shock dynamics studies. In comparison with inert Euler simulations, we find that GSD perturbations have a longer wavelength. However, by adjusting the oscillation period to match the Euler simulations and applying the linear decay law, we achieve good agreement with the observed decay. Finally, experimental validation of the scaling law is crucial for confirming its accuracy. Future experimental work will allow for direct comparison with simulations and refine the models. A key challenge remains predicting the wavelength, which is vital for understanding shock wave dynamics.

Acknowledgements

We acknowledge financial support from the French Alternative Energies and Atomic Energy Commission (CEA) for the grant "Decay of non-uniform shocks and their reflection in reactive gases".

References

[1] R. M. Bowman, "Investigation of shock front topography in shock tubes," Ph.D. dissertation, California Institute of Technology, 1966.

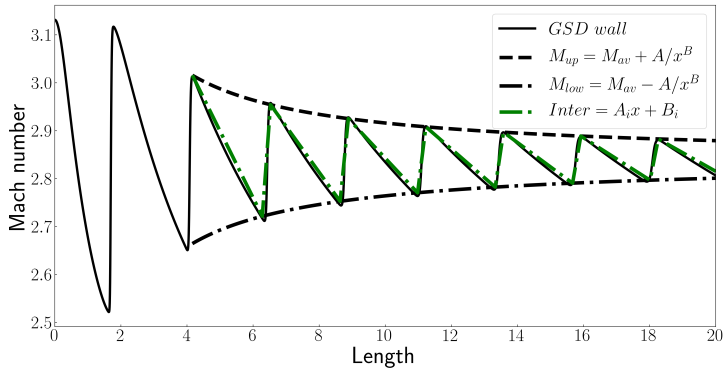

Figure 4: Global and internal decay of shock perturbations. Proposed linear decay in green.

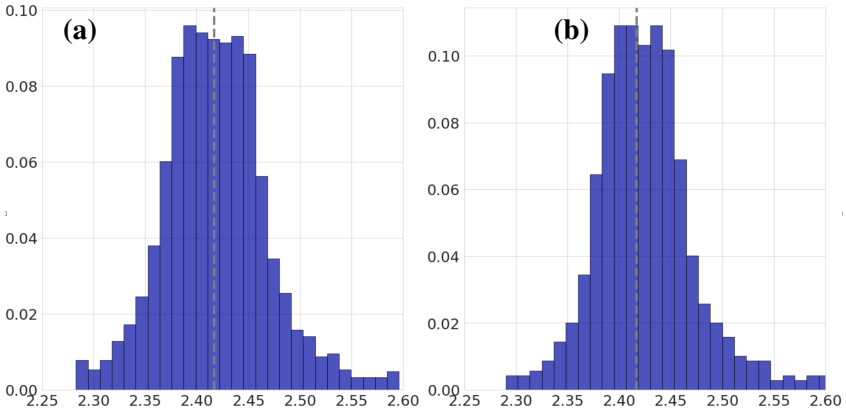

Figure 5: Probability density function: a) GSD and b) Proposed Linear decaying wave.

[2] N. C. Freeman, "A theory of the stability of plane shock waves," *Proceedings of the Royal Society of London. Series A. Mathematical and Physical Sciences*, vol. 228, no. 1174, pp. 341–362, 1955.

[3] Y. Zhang, J. F. Zou, and Y. Zheng, "Comparative analysis of flow behind a normal shock wave reflected off a wavy end-wall at different mach numbers and wave amplitudes," *Shock Waves*, vol. 32, no. 2, pp. 179–194, 2022.

[4] G. Lodato, L. Vervisch, and P. Clavin, "Direct numerical simulation of shock wavy-wall interaction: analysis of cellular shock structures and flow patterns," *Journal of Fluid Mechanics*, vol. 789, p. 221–258, 2016.

[5] P. Clavin, "Nonlinear analysis of shock–vortex interaction: Mach stem formation," *Journal of Fluid Mechanics*, vol. 721, p. 324–339, 2013.

[6] G. Lodato, L. Vervisch, and P. Clavin, "Numerical study of smoothly perturbed shocks in the newtonian limit," *Flow, Turbulence and Combustion*, vol. 99, no. 3, pp. 887–908, 2017.

[7] G. Whitham, *Linear and Nonlinear Waves*. Wiley, 1999.

[8] W. Mostert, D. I. Pullin, R. Samtaney, and V. Wheatley, "Geometrical shock dynamics for magnetohydrodynamic fast shocks," *Journal of Fluid Mechanics*, vol. 811, p. R2, 2017.

[9] D. W. Schwendeman, "A new numerical method for shock wave propagation based on geometrical shock dynamics," *Proceedings of the Royal Society of London. Series A: Mathematical and Physical Sciences*, vol. 441, no. 1912, pp. 331–341, 1993.